2D and 3D Cu/ Zn order-disorder transitions in Cu_2ZnSnS_4 from Monte Carlo simulations

Suzanne K. Wallace,[a,b] Jarvist Moore Frost,[c] and Aron Walsh*[b,d]

[a] *Department of Chemistry, Centre for Sustainable Chemical Technologies, University of Bath, Claverton Down, Bath, BA2 7AY, UK*

[b] *Department of Materials, Imperial College London, Exhibition Road, London SW7 2AZ, UK. Email: a.walsh@imperial.ac.uk*

[c] *Department of Physics, King's College London, Strand, London WC2R 2LS, UK*

[d] *Department of Materials Science and Engineering, Yonsei University, Seoul 03722, Korea*

Received Xth XXXXXXXXXX 20XX, Accepted Xth XXXXXXXXX 20XX

First published on the web Xth XXXXXXXXXX 200X

DOI: 10.1039/b000000x

Kesterite-structured Cu_2ZnSnS_4 (CZTS) is an earth-abundant and non-toxic semiconductor that is being studied for use as the absorber layer in thin-film solar cells. Currently the power-conversion efficiencies of this technology fall short of the requirements for commercialisation, despite the promising sunlight-matched optical band gap. Disorder in the Cu-Zn sub-lattice has been observed and is proposed as one possible explanation for the shortcomings of CZTS solar cells. Cation site disorder averaged over a macroscopic sample does not provide insights into the microscopic cation distribution that will interact with photogenerated electrons and holes. To provide atomistic insight into Cu-Zn disorder we have developed a Monte Carlo (MC) model based on pairwise interactions and parameterised with the dielectric constant of CZTS calculated from first principles. Substitutional disorder amongst in-plane Cu and Zn ions on the 2*c* and 2*d* Wyckoff sites, i.e. 2D disorder, has been proposed as the dominant form of Cu/ Zn disorder. We use our model to study the Cu/ Zn order-disorder transition (ODT) in 2D but also allow Zn to substitute onto the Cu 2*a* site, i.e. 3D disorder. We find that Zn ions readily substitute onto the Cu 2*a* site and that the critical temperature for the ODT for 3D disorder is lower than that for 2D Cu/ Zn disorder and closer to the temperatures reported from experimental works.

1 Introduction

Amongst the semiconductors being developed for applications in thin-film photovoltaic (PV) devices, kesterite-structured Cu_2ZnSnS_4 (CZTS) stands out as being composed of low-cost, earth-abundant and non-toxic elements. While the material has many of the bulk properties required to be a high-efficiency photovoltaic absorber, such as a high absorption coefficient of $10^4 cm^{-1}$ and a direct band gap of 1.5 eV[1], the power-conversion efficiencies (PCEs) of solar cells are considerably less than the theoretical maximum of 28% as predicted by the Shockley-Queisser limit[2] based on its sunlight-matched optical band gap. The current confirmed record PCE for the kesterite-based alloy $Cu_2ZnSn(S_xSe_{1-x})_4$ (CZTSSe) is at 12.6%[3], while that of the pure sulfide material still lags behind at 11%[4], both of which are far below that of the similar PV technology $Cu(In_{1-y},Ga_y)Se_2$ (CIGSe) with a record PCE of 22.6%[5].

The low open-circuit voltage (compared to the optical band gap) limits achieved device efficiencies[6,7]. This is referred to as the V_{OC} deficit. It is possible that the efficiency of devices fabricated with absorber layers produced from different synthesis procedures may be limited by different factors, making it a difficult task to pinpoint a universal origin of the V_{OC} deficit in CZTS solar cells. Defects and bulk disorder in CZTS is one possible explanation for the V_{OC} deficit[8,9]. For record-efficiency devices, produced by the hydrazine-based solution method pioneered at the IBM T. J. Watson Research Center[3,10], this has been attributed to fluctuations in electrostatic potential due to Cu-Zn disorder, and associated band tailing[11]. The origin of the V_{OC} deficit is still an on-going debate[6].

Substitutional disorder within the cation sublattice of tetrahedrally bonded multinary semiconductors is a particularly likely form of disorder[12]. This can decisively alter the electronic properties of a material[13]. Substitutional disorder between Cu^+ and Zn^{2+} ions has a low enthalpic cost due to the similar ionic radii and chemical character of the two species. Density functional theory (DFT) predicts a low formation energy for the $[Cu^-_{Zn} + Zn^+_{Cu}]$ antisite defect pair[14] and there is a large body of evidence for the presence of disorder amongst Cu^+ and Zn^{2+} ions in CZTS[15–20]. Furthermore, Ref. 18–21 indicate a distinct order-disorder transition (ODT) attributed to Cu-Zn substitutional disorder.

During the high-temperature synthesis of CZTS disorder

can be 'frozen in' to the material as it cools to room temperature. Studies have been conducted to determine if low temperature post-deposition annealing could improve device performance and some improvements were observed from such treatments[22,23]. However, in the latter study the authors postulate that a high level of order amongst the Cu^{+} and Zn^{2+} ions would require years of this treatment[23]. It is unclear if the disorder is due to slow kinetics, which could possibly be improved through optimising the processing conditions, or if the disorder is due to fundamental thermodynamic limitations for the material at room temperature[24]. In our study, we model only thermodynamic equilibrium disorder as a function of temperature. Therefore, our model could be used to isolate disorder due to equilibrium thermodynamics from kinetic limitations in experiments. Our model can be used to quantify the absolute limit on order in Cu_2ZnSnS_4 at experimentally relevant temperatures and to generate atomic configurations arising from the disorder process.

Devices made from an alloy of Cu_2ZnSnS_4 and $Cu_2ZnSnSe_4$, i.e. $Cu_2ZnSn(S_xSe_{1-x})_4$, make the highest performing devices[3,10]. In this study we focus on the pure sulfide. The V_{OC} deficit is worse in CZTS devices[6] and so potentially studying causes of the problem in this particular system could be more informative. Although ultimately the aim for this technology is to make thin-film devices from CZTS, in which the material is likely to be polycrystalline with grain boundaries, we focus on the bulk material. We are doing this for two reasons. Firstly, to improve the understanding of the fundamental material properties before attempting to understand a more complex system. Secondly, it has been proposed that the V_{OC} deficit in CZTSSe devices could be associated with properties of the bulk crystal[25]. It is believed that the most recent high-performance devices are not limited by interface recombination[26,27]. Furthermore, devices fabricated from single crystals have demonstrated a V_{OC} deficit of 530 mV, which equals that of the record thin-film devices, indicating that the deficit could largely be due to bulk disorder[28].

Studies on various multinary semiconductors have indicated that it is not sufficient to consider only point defects to understand the defect physics of this type of compound due to the likely presence of structural disorder and extended antisite defects, which can dramatically lower the formation energy of defects[12,29]. System sizes that avoid artificial periodic disorder and associated finite-size effects would be beyond computationally feasible limits for density functional theory (DFT) or other first-principles calculations. However, some studies have investigated substitutional disorder through Metropolis Monte Carlo (MC) simulations of the redistribution of local structural motifs centred on the S-ions in CZTS, with energies calculated by DFT, out to nearest-neighbour interactions[29,30] and another study has been carried out using a cluster expansion of interacting dimers and trimers in CZTS[24], for system sizes of 1200 atoms and 512 atoms respectively. Prior to these studies there has been little work modelling disordered phases in CZTS, apart from one study where the choice of the disordered phase was arbitrary[31] and another investigating the configurational entropy of possible independent microstates in systems of up to 64 atoms[32].

In this study, we simulate substitutional disorder between Cu^{+} and Zn^{2+} ions for system sizes of over 10,000 atoms. We use on-lattice Metropolis MC simulation with a classical interatomic interaction model tha has been parameterised the the dielectric constant of CZTS calculated from first principles[41] to calculate changes lattice energies when performing Cu-Zn substitutions. Our model allows us to freeze certain species in the system, we are therefore able to study separately thermodynamic disorder in 2D where substitutions are only in-plane between Cu and Zn ions on 2*c* and 2*d* sites and thermodynamic disorder in 3D where Zn may also subsitute on the Cu 2*a* sites. Cu/ Zn disorder in 2D (between 2*c* and 2*d* sites) is believed to be the most prevalent type of substitutional disorder for near stoichiometric samples but that substitions onto the Cu 2*a* sites may become possible after the Cu/ Zn order-disorder transition (ODT) has occurred from substitutions between the 2*c* and 2*d* sites[18]. However recent studies have suggested that disorder is also prevalent on the 2*a* site and that this plays an important role in the ODT[33,34]. We therefore perform simulations to study the order-disorder transition (ODT) for both cases. We develop methods to ensure that the equilibrium disordered configuration has been reached at each simulation temperature and assess finite-size effects in the model on the disorder process. Tools are developed to quantify the structural disorder in the equilibrated configurations that are obtained. We finish with the temperature dependence of thermodynamic Cu-Zn order in our model of CZTS and show the spatial distribution of antisites at various temperatures. Simulations are performed in parallel over different temperatures using GNU parallel[35], and the associated simulation codes have been made openly available.

2 Computational Methodology

2.1 Lattice model of Cu_2ZnSnS_4

The crystal structure of Cu_2ZnSnS_4 can be described by two inter-pentrating face-centred cubic (FCC) lattices: one of metal cations and one of sulfur anions. This is shown in Figure 1a, where green planes are a guide to the eye to distinguish the anion sub-lattice. We consider the sulfur sub-lattice to be invariant as any substitution between ions in the cation sublattice and sulfur anion sub-lattice would be energetically infeasible. The sulfur sub-lattice is implicit during the MC simulations but incorporated later in calculations of lattice elec-

trostatics. The cation lattice can be described by alternating layers of Cu-Sn and Cu-Zn in (001) planes, as shown in Fig. 1b. Cu/ Zn disorder in only the Cu-Zn (001) planes is referred to as '2D disorder' in this study, while full Cu/ Zn disorder is referred to as '3D disorder'. In the case of the latter, Zn ions are able to substitute onto Cu 2*a* sites in the Cu-Sn (001) planes. For computational convenience, we map this FCC lattice onto a simple cubic (SC) lattice for our simulations by introducing empty lattice sites.

The separation between lattice sites in our model is re-scaled using DFT (PBEsol functional) optimised lattice parameters of $a = b = 5.44$ Å[37]. Kesterite has a tetragonal lattice with a $\frac{c}{2a}$ ratio close to 1 (0.998 from DFT/PBEsol-optimisation). We use a value of 1 in the MC simulations, which has a minor effect on the lattice energy as confirmed from explicit calculations using the General Utility Lattice Program (GULP)[38]. Lattice energies of an ordered 64 atom supercell with the exact DFT/PBEsol-optimised lattice parameters and an equivalent supercell with the approximated lattice parameters differed by less than 2%.

In our model we fix the position of Sn ions. To simulate only nearest-neighbour Cu-Zn disorder within the Cu-Zn layers, we use a cut-off radius of 2 lattice units (to account for the empty sites between each cation, shown in Fig. 4). The cut-off radius in the *c*-direction is only 1 lattice unit so that substitutions may only occur with the plane above or below. The model does not account for strain effects during Cu-Zn substitutions as it is fixed on-lattice. It has been reported that there is a small change in the *c* lattice parameter with increased disorder[39]; however, due to the similar ionic radii of Cu and Zn we neglect this effect, but it could be incorporated into future models. Our model also does not allow for any displacement of S ions from Cu-Zn substitutions. Sn ions have the largest formal charge in the lattice and are fixed during the simulations. We therefore expect the stationary cation backbone of the lattice to be dominant in determining the position of the S anions and therefore expect displacements due to Cu-Zn disorder to be very small.

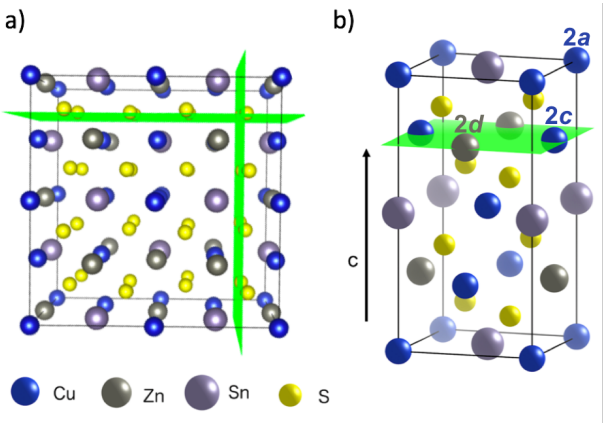

Fig. 1 Representations of the crystal structure of kesterite-structured Cu_2ZnSnS_4 where green planes are used as guides to the eye: a) supercell indicating the two inter-penetrating anion and cation sub-lattices, b) the conventional unit cell highlighting a Cu-Zn layer in the (001) planes along the *c*-axis. Visuals were produced using VESTA[36].

2.2 Pair interaction model and Metropolis Monte Carlo simulation of cation disorder

The MC method can be used to calculate thermodynamic information about a system of interacting ions, which we represent on a 3D lattice as described above. We assume that the potential field of an ion is spherically symmetric and consider two-body forces acting between all pairs of ions in this system. If we know the positions of the N interacting ions on the lattice then the potential energy of the system can be calculated using equation 1, where d_{ij} is the minimum distance between ions i and j with charge q_i and q_j[40].

$$U = \frac{1}{2}\sum_{i=1}^{N} q_i \sum_{j=1}^{N(j\neq i)} \frac{1}{4\pi\varepsilon_0}\frac{q_j}{d_{ij}} \tag{1}$$

To calculate the properties of the system, the canonical (NVT) ensemble is used where the number of ions, volume and temperature are all constant. The trial MC moves are swaps between nearest-neighbour Cu and Zn ions.

Using a standard MC method for our system would involve placing each of the N ions at random positions in the lattice to define a random point in the $3N$-dimensional configuration space. However, most configurations are improbable so performing this calculation for every possible configuration would be inefficient and unnecessary to sufficiently evaluate the ensemble. The custom MC code in this study makes use of the Metropolis modified MC scheme[40]. In this implementation of the MC method, instead of choosing configurations randomly and then weighting them, the Metropolis algorithm considers the relative probability of a system being in a new configuration, β, to that of being in the current configuration, α. This is shown in equation 2, where E_α is the energy of state α, E_β is the energy of state β, and Z is the partition function. For most systems, calculating the value of the partition function requires the summation over a large number of states. However, within the Metropolis scheme, in the expression for the probability of the trial Z cancels out.

$$\frac{p_\beta}{p_\alpha} = \frac{e^{-\frac{E_\alpha}{k_b T}}}{Z}\frac{Z}{e^{-\frac{E_\alpha}{k_b T}}} = e^{-\frac{E_\beta - E_\alpha}{k_B T}} \tag{2}$$

The relative probabilities of the two states are completely de-

termined by the energy difference, such that if:

$$\Delta E = E_\beta - E_\alpha \leq 0, \text{ then } \frac{p_\beta}{p_\alpha} \geq 1 \quad (3)$$

and if

$$\Delta E = E_\beta - E_\alpha > 0, \text{ then } \frac{p_\beta}{p_\alpha} < 1 \quad (4)$$

It is then decided if this new configuration should be added to the trajectory of the system (towards the minimum energy configuration), or not, based on the probability of the new configuration relative to the current configuration. If the relative probability is ≥ 1, as shown in equation 3, then the move is accepted and added to the trajectory. However, if the relative probability is < 1 then the move will only be accepted if $e^{-\frac{\Delta E}{k_B T}} \geq$ a random number generated between 0 and 1.

Lattice energy summations of the system were performed before and after a proposed Cu-Zn substitution out to a finite radius to obtain ΔE. Within periodic boundary conditions, the upper limit for the cut off radius is half the minimum dimension of the system. Details of the convergence in ΔE with respect to the cut off radius used in the lattice summations are given in the SI. Equation 5 is used to calculate the electrostatic interaction between pairs of ions in the system, where q_1 and q_2 are the bare formal charges, r is the separation of the point charges, ε_r is the effective dielectric constant of the crystal and ε_0 is the permittivity of free space.

$$E_{electrostatic} = \frac{q_1 q_2}{4\pi\varepsilon_0\varepsilon_r} e^2 \frac{1}{r} = q_1 q_2 I_{electrostatic} \quad (5)$$

To calculate a value of $I_{electrostatic}$ to use in our MC model, we use the separation of nearest-neighbour Cu-Zn ions for r (3.8 Å) and the calculated value for the static dielectric constant of perfect single crystal CZTS of 9.9[41]. This results in $I_{electrostatic}$ = -0.378 eV for our model.

3 Results and discussion

3.1 Equilibration

Due to the stochastic nature of the trajectory from an initial configuration in the MC method, we cannot draw any conclusions about the equilibrium thermodynamic properties of that system at the given simulation temperature until equilibrium has been reached. The number of simulation steps required to reach this point is the 'equilibration time'. Equilibration is often considered as the point at which the value of a quantity of interest, which initially changes by a large amount, eventually converges to fluctuating about a steady average value. This is dependent upon the principle that a system in equilibrium spends the majority of time in a small subset of states in which the properties take a narrow range of values[43].

Our MC model for Cu-Zn disorder is analogous to the Ising model of a ferromagnet and we describe the rationale for our equilibration procedure by referring to this common example. In the case of an Ising model, the trial moves in the Metropolis algorithm are spin flips, whereas in our model the trial moves are swaps between Cu and Zn ions. For the Ising model, one MC step corresponds to attempting a trial spin-flip at all sites in the system once. Similarly, for our model one MC step corresponds to sweeping across the entire lattice and attempting a near-neighbour Cu-Zn swap at each Cu and Zn site. In the case of the Ising model it is usually the average magnetisation of the system, or internal energy, as a function of temperature that are the quantities of interest. For our system, we are interested in the configuration of the ions (and extent of thermodynamic disorder) and the corresponding distribution of the electrostatic potential across the system, as this can be related to the observed band tailing. We now explore two methods to gauge when the system has reached the equilibrium disordered configuration at each simulation temperature: the pair correlation function (PCF) for information on the structural disorder and also the variance of the distribution of on-site electrostatic potentials of species in the system.

3.1.1 Pair correlation functions from ordered and disordered initial lattices We first attempted two simulations for each temperature, one starting from an initial ordered lattice and one from an initial disordered lattice (produced by randomly 'shuffling' Cu and Zn ions in the ordered lattice), until both simulations converged to the same equilibrium configuration. To gauge the point at which this had been reached, we compare the pair correlation functions (PCFs) for each configuration, an example of this analysis is given in Fig. 2.

We found that systems initialised from a disordered lattice required a substantially larger number of MC steps to evolve away from the initial configuration. This can be seen in Fig. 2 from the Zn-Zn PCFs. The most noticeable feature when comparing the PCF for an ordered initial lattice to that of a disordered lattice is the emergence of a new nearest-neighbour Zn-Zn peak at $\sqrt{2}$ due to the clustering of Zn ions once Cu and Zn ions have been allowed to substitute. This point is discussed further in section 3.2 as an order parameter, but for now we just remark that the peak is largest for the disordered initial lattice and decreases for the system evolved from this initial configuration at moderate simulation temperatures. After a considerably large number of MC steps the peak for the two systems evolved from the ordered and disordered initial lattices were not of the same height. This observation may be explained by the entropic penalty in going from a disordered to a more ordered system, suggesting that this method may not be computationally efficient. We therefore adopted an alternative approach to check for equilibration, as outlined below.

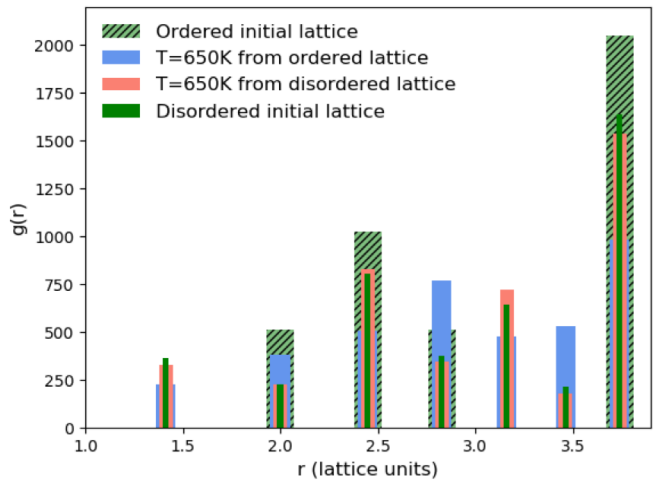

Fig. 2 The pair correlation function (PCF) between pairs of Zn ions in Cu_2ZnSnS_4. PCFs of an initial ordered lattice are plotted with that of a disordered initial lattice as reference points as well as systems that have been evolved from both of these initial configurations at T = 650 K. Widths of the bars plotted are arbitrarily chosen to ensure all data is visible.

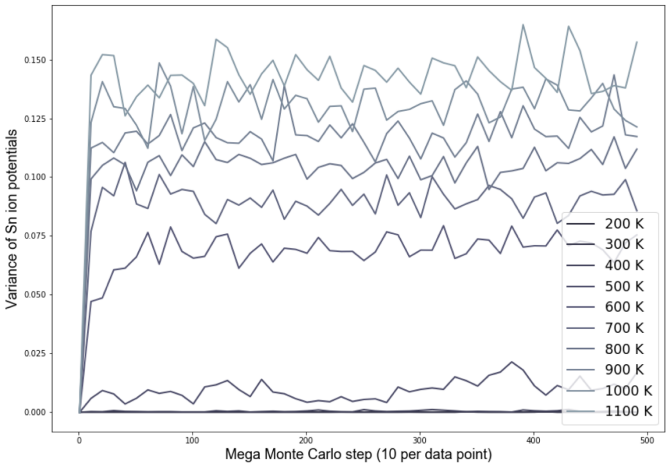

Fig. 3 Variance in the distribution of the on-site electrostatic potential of Sn ions in a 24×24×24 Cu_2ZnSnS_4 system (containing 13,824 ions in total) across a range of simulation temperatures with 3D Cu/ Zn disorder. Equivalent for 2D disorder can be found in the SI. Each mega Monte Carlo step corresponds to sweeping across the lattice and attempting 100 trial moves per lattice site.

3.1.2 Variance in the distribution of on-site electrostatic potentials Our second method is analogous to using the point at which the average magnetisation fluctuates about a steady value in the Ising model, as discussed earlier. We check the number of MC steps required for the variance of the distribution of on-site electrostatic potentials of all Sn ions in the lattice to fluctuate about a steady value. We use Sn ions because we have fixed the locations of Sn ions in our simulations, making them stationary reference points. There is one crystallographically distinct Sn lattice site in Cu_2ZnSnS_4. We start from an ordered lattice and as all ions are on their correct lattice sites, there is only one unique chemical environment for Sn and the variance in electrostatic potential is zero. As the system evolves, and Cu and Zn ions are substituted, unique chemical environments emerge for the Sn ions in the system.

An example of a test to determine a suitable number of MC steps for equilibration (i.e. steps to run before collecting data on the system) is shown in Fig 3 for 3D Cu/ Zn disorder. The equivalent for 2D disorder is given in the SI. We perform this check for the largest system size in our study and the whole simulation temperature range we study. A larger system may require a considerably larger number of MC steps to equilibrate and we perform the check for each temperature because if there is a phase transition (as suggested in several works [18–21]), there could be 'critical slowing down' close to the transition temperature.

From Fig. 3, we take 200 mega MC steps as a suitable number of equilibration steps to ensure all simulation temperatures have reached their equilibrium configuration before we start collecting data. One mega MC step consists of attempting on average 100 trial Cu-Zn substitutions per site per data point, i.e. 100 sweeps of the lattice per mega MC step. The absence of variance in Fig. 3 when the simulation temperature is at 0 K is because the system remains ordered.

3.2 Order parameters

To quantify the extent of substitutional Cu-Zn disorder in our system, we consider two order parameters to enable us to investigate long- and short-ranged order.

3.2.1 Pair correlation functions Pair correlation functions (PCFs) show the number of pairs of particular species with particular separations within the system. We generate reference PCFs of ordered and disordered systems (using equilibrated configurations at low and high temperatures, respectively) of the same size. The most noticeable feature in the PCFs of the system was the emergence of a new nearest-neighbour peak in the Zn-Zn PCF at $\sqrt{2}$. This can be explained using Fig. 4. In the ordered lattice the shortest Zn-Zn spacing is 2 lattice units. Once Cu and Zn begin to substitute a new shortest Zn-Zn spacing of $\sqrt{2}$ lattice units becomes possible. An increase in the intensity of this $\sqrt{2}$ peak indicates more clustering of Zn ions and so provides insights into the extent of short-ranged disorder in the system. The same analysis is not possible using the Cu-Cu PCF because a $\sqrt{2}$ Cu-Cu separation is present between the (001) planes in the ordered lattice.

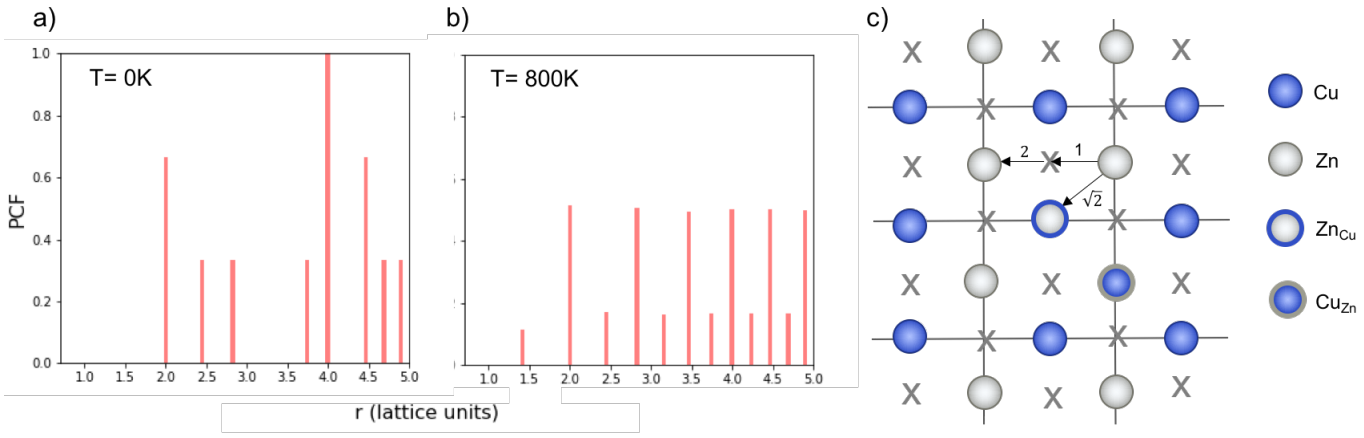

Fig. 4 Normalised Zn-Zn pair correlation functions (PCFs) at 0K (a) and 800K (b) for an (001) Cu-Zn plane in the cation sub-lattice of Cu_2ZnSnS_4 with structure shown in (c). Crosses denote the gap sites used in our lattice model to map an fcc lattice onto a sc lattice. Before a Cu-Zn swap, the nearest-neighbour Zn-Zn pair is 2 lattice units apart. After a Cu-Zn swap there is a Zn-Zn pair separated by r=$\sqrt{2}$. The 0K PCF is for the perfectly ordered lattice before any Cu-Zn substitutions have occurred and shows a Zn-Zn PCF peak intensity of zero at r=$\sqrt{2}$. The 800K PCF shows an increase in the peak intensity at r=$\sqrt{2}$, once Cu and Zn ions begin to substitute.

3.2.2 Cation site occupancy An order parameter used in experimental literature to quantify Cu-Zn disorder in kesterite-structured Cu_2ZnSnS_4, $Cu_2ZnSnSe_4$ and $Cu_2ZnSn(S_xSe_{1-x})_4$ is based on cation site occupancies [18,19]. In ordered CZTS, Cu ions occupy 2*c* sites in the Cu-Zn layers indicated in Fig. 1b and 2*a* sites in the Cu-Sn layers. Sn ions occupy the 2*b* sites and Zn ions occupy the 2*d* sites [21]. In completely disordered CZTS Cu and Zn are found evenly distributed over 2*c* and 2*d* sites, indicating disorder in the Cu-Zn layers. A measure of increasing order is when Cu shows a preference to occupy 2*c* sites and Zn to occupy 2*d* sites. For ordered CZTS, the parameter $S = 1$, corresponding to all Zn ions on 2*d* sites and all Cu ions on 2*c* sites. For fully disordered CZTS $S = 0$, corresponding to no preference for Cu or Zn to occupy their ideal crystallographic site.

$$S = \frac{[Cu_{2c} + Zn_{2d}] - [Zn_{2c} + Cu_{2d}]}{[Cu_{2c} + Zn_{2d}] + [Zn_{2c} + Cu_{2d}]} \quad (6)$$

However, it is possible that this metric may overestimate the extent of disorder in a system as locally ordered domains, displaced relative to the configuration of the initial lattice, would be considered as disordered. We therefore compare the extent of order at each simulation temperature inferred from our PCF analysis to that suggested by the *S* parameter as we increase the system size to check for the formation of locally ordered domains. A decrease in *S* and an increase in Zn-Zn PCF $\sqrt{2}$ peak intensity correspond to a reduction in order in the system. For the case of locally ordered domains, a low *S* (suggesting large extents of Cu-Zn disorder) could coincide with a relatively small $\sqrt{2}$ Zn-Zn PCF peak, suggesting long-range disorder, but short range order within the Cu-Zn planes. It is also worth noting that the S order parameter only considers disorder on the 2*c* and 2*d* sites and hence neglects disorder on the Cu 2*a* when 3D Cu/ Zn disorder is present. However, the use of the first Zn-Zn PCF peak as an order parameter is also valid when considering 3D disorder as substitutions of Zn onto the 2*a* can result in Zn ions being separated by $\sqrt{2}$ lattice units.

3.3 Finite size effects

To investigate finite size effects, we perform simulations for system sizes ranging from 12×12×12 (= 1,728 ions) to 32×32×32 (= 32,768 ions). We investigate the disorder behaviour of the systems as a function of temperature using the two order parameters in Fig. 5. Fig. 5a shows the increase in the intensity of the Zn-Zn PCF at $r = \sqrt{2}$ with temperature (explained schematically in Fig. 4. Fig. 5b shows the decrease in *S* from 1 to 0 with increased simulation temperature. Both order parameters show approximately the same disorder temperature. Our model shows clear signs of finite size effects for the smallest systems, in the regime used in previous studies. We consider a 24×24×24 size system (= 13,824 ions) to give a converged disorder process with respect to system size and use this system size for all subsequent simulations.

3.4 Cu/ Zn order-disorder transitions

In this section we use the order parameters introduced in section 3.2 to characterise the Cu/ Zn order-disorder transitions (ODTs) for 2D Cu/ Zn disorder (when the only mechanism is substitutions between Cu and Zn ions on 2*c* and 2*d* sites)

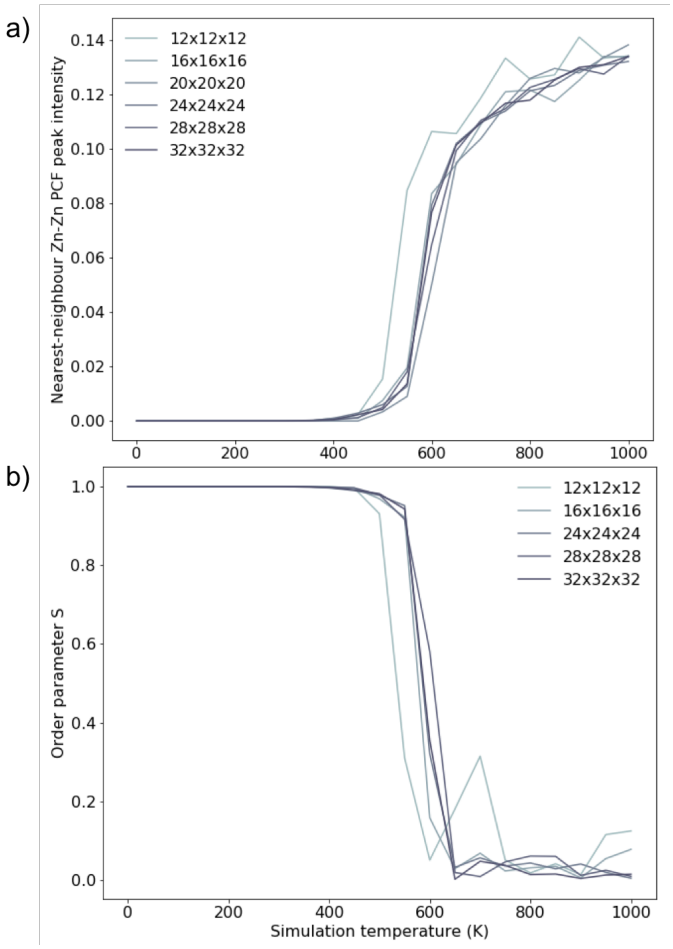

Fig. 5 Two order parameters to assess finite-size effects for 3D Cu/ Zn disorder. Equivalent for 2D disorder can be found in the SI. (a) The nearest-neighbour ($r = \sqrt{2}$) Zn-Zn pair correlation function peak intensity for systems of various sizes at thermodynamic equilibrium across simulation temperatures ranging from 0 to 1000 K, indicating clustering of Zn ions and deviation from the perfectly ordered lattice with a $r = \sqrt{2}$ peak intensity greater than zero. (b) The S order parameter based on Cu and Zn site occupancies in Cu_2ZnSnS_4 as a function of simulation temperature. $S = 1$ corresponds to a fully ordered lattice and $S = 0$ corresponds to complete Cu-Zn disorder within the (001) plane. (b).

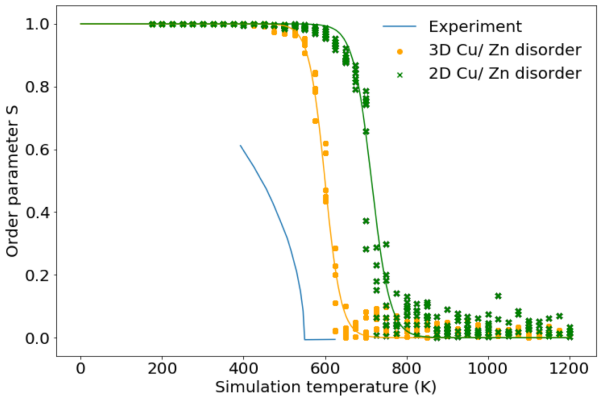

Fig. 6 The S order parameter based on Cu and Zn site occupancies in Cu_2ZnSnS_4 for $24\times24\times24$ (= 13,824 ions) from 11 independent Monte Carlo simulations for 2D Cu/ Zn disorder and 3D Cu/ Zn disorder plotted against anomalous X-ray powder diffraction data for $Cu_2ZnSnSe_4$ from Ref. 18. Experimental data has been shifted by 70K to account for the difference in the order-disorder transition temperature for the pure sulfide and pure selenide reported in Ref. 44.

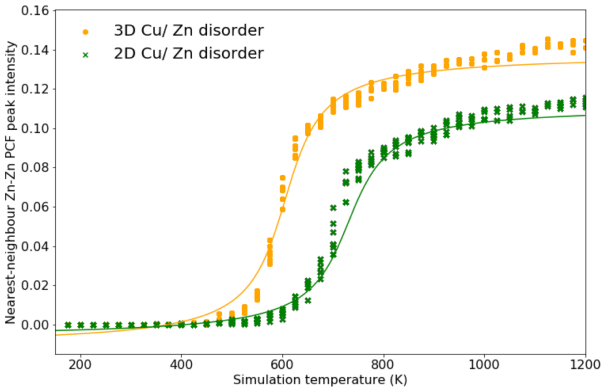

Fig. 7 The nearest-neighbour Zn-Zn pair correlation function peak intensity, which emerges due to the substitution of Zn ions onto nearest-neighbour Cu sites in Cu_2ZnSnS_4 as shown in Fig. 4. 11 independent Monte Carlo simulations are performed for 2D Cu/ Zn disorder and 3D Cu/ Zn disorder.

and for 3D Cu/ Zn disorder (when Zn may also substitute onto the Cu 2a sites). To improve our statistics, we performed 11 independent Monte Carlo simulations, each using different random number seeds and perform simulations across smaller temperature increments at temperatures close to the ODT critical temperatures, T_C, for 2D and 3D Cu/ Zn disorder. Due to the possibility of critical slowing down when using temperature increments closer to T_C, we repeat equilibration checks to ensure data is still for equilibrated configurations.

Fig. 6 compares the S order parameter based on the cation occupancy of 2c and 2d sites obtained for simulations of both 2D and 3D Cu/ Zn disorder to anomalous X-ray powder diffraction data for $Cu_2ZnSnSe_4$ from Ref. 18. In the plot, experimental data has been shifted by 70K to account for the difference in the order-disorder transition temperature for the pure sulfide and pure selenide reported in Ref. 44. As our model considers only thermodynamic disorder, the difference in the value of the S order parameter at comparable temperatures between our model and experiment and the diverging gradients of the curves at lower temperatures could be

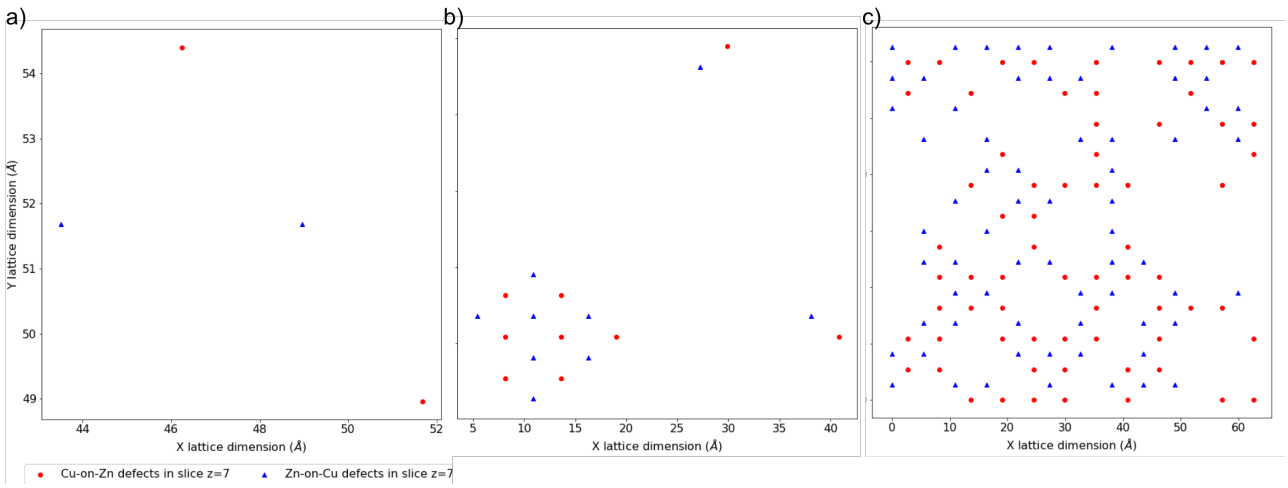

Fig. 8 24×24×24 ions system with 2D Cu/ Zn disorder. Critical temperature, T_c, for the order-disorder transition is approximately 800K for this system. (a) shows antisite locations at T=550K in a Cu-Zn plane, (b) shows the same plane at T=650K with the formation of a distinct disordered region and c) shows the same plane above T_c at T=900K.

attributed to kinetic limitations on the ordering processes that will be present in the real system but not in our model. T_C from the *S* order parameter corresponds to the temperature after which $S = 0$. Fig. 6 shows a T_C of approximately 800K and 650K for 2D and 3D Cu/ Zn disorder respectively. T_C predicted from our model using the *S* order parameter is closer to the experimental value of approximately 550K for 3D Cu/ Zn disorder. The larger T_C of our model than experimental values could be due to our use of the calculated dielectric constant for the perfect, bulk crystal to parameterise the interaction energy, as outlined at the end of section 2.2. The perfect, bulk dielectric constant may be slightly smaller than that of a real, polycrystalline system and hence the interaction parameter in Eq. 5 as used in our model may be overestimated. In a polycrystalline thin-film there may be additional contributions to dielectric polarisation from the presence of internal interfaces and inhomogeneity in the electrical properties[42], which will not be accounted for in the calculated dielectric constant for the bulk crystal.

As discussed in section 3.2, the *S* order parameter only accounts for Cu/ Zn disorder on the 2*c* and 2*d* sites and therefore may miss some disorder in the 3D case. For this reason, the nearest Zn-Zn PCF peak order parameter is also used to compare to ODT for 2D and 3D Cu/ Zn disorder. The high-temperature Zn-Zn nearest-neighbour PCF peaks shown in Fig. 7 can be understood as the Cu-Zn planes beginning to melt. Within the cation sub-lattice, there are 12 sites $\sqrt{2}$ apart. In the $S = 0$ disorder regime, Cu shows no preference to occupy the *2c* sites and Zn to occupy the *2d* sites, we can therefore expect the density of Zn $\sqrt{2}$ away from every other Zn to converge towards 2/12 (approximately 0.167). However, we cannot expect the PCF peak at high-temperatures to reach a complete plateau at high-temperatures as is seen for the *S* order parameter due to the lower stoichiometric ratio of Zn relative to Cu in Cu_2ZnSnS_4. The larger PCF peak intensity for 3D Cu/ Zn disorder than for 2D Cu/ Zn disorder can be understood by the larger number of possible options for Zn to substitute onto nearest-neighbour Cu sites in the 3D case.

Fig. 8 and 9 show locations of Cu-on-Zn and Zn-on-Cu antisites in Cu-Zn and Cu-Sn (001) planes of the lattice model at various simulation temperatures for 2D and 3D Cu/ Zn disorder respectively. In each case, the choice of planes used for the visualisation was chosen based on ones that showed the presence of disorder in the low-disorder temperature regime when disorder was not present in all layers of the lattice. Fig. 8a and b show two configurations at temperatures below T_C for the 2D Cu/ Zn ODT where Fig. 8b shows the formation of a distinct disordered region in the lower left corner of the plane. Fig. 8c shows a configuration above T_C with a large extent of Cu/ Zn disorder. Fig. 9a and b show the location of a small number of Cu-on-Zn and Zn-on-Cu antisites in the Cu-Zn and Cu-Sn (001) planes respectively at a simulation temperature below T_C for the 3D Cu/ Zn ODT. It can be seen here that Zn readily subsitutes onto the Cu 2*a* sites even in this low-disorder temperature regime. Fig. 9c and d show the antisite locations in the same planes at a simulation temperature above T_C for the 3D Cu/ Zn ODT, which shows a similar spatial distribution of antisites to that observed for 2D Cu/ Zn disorder above T_C.

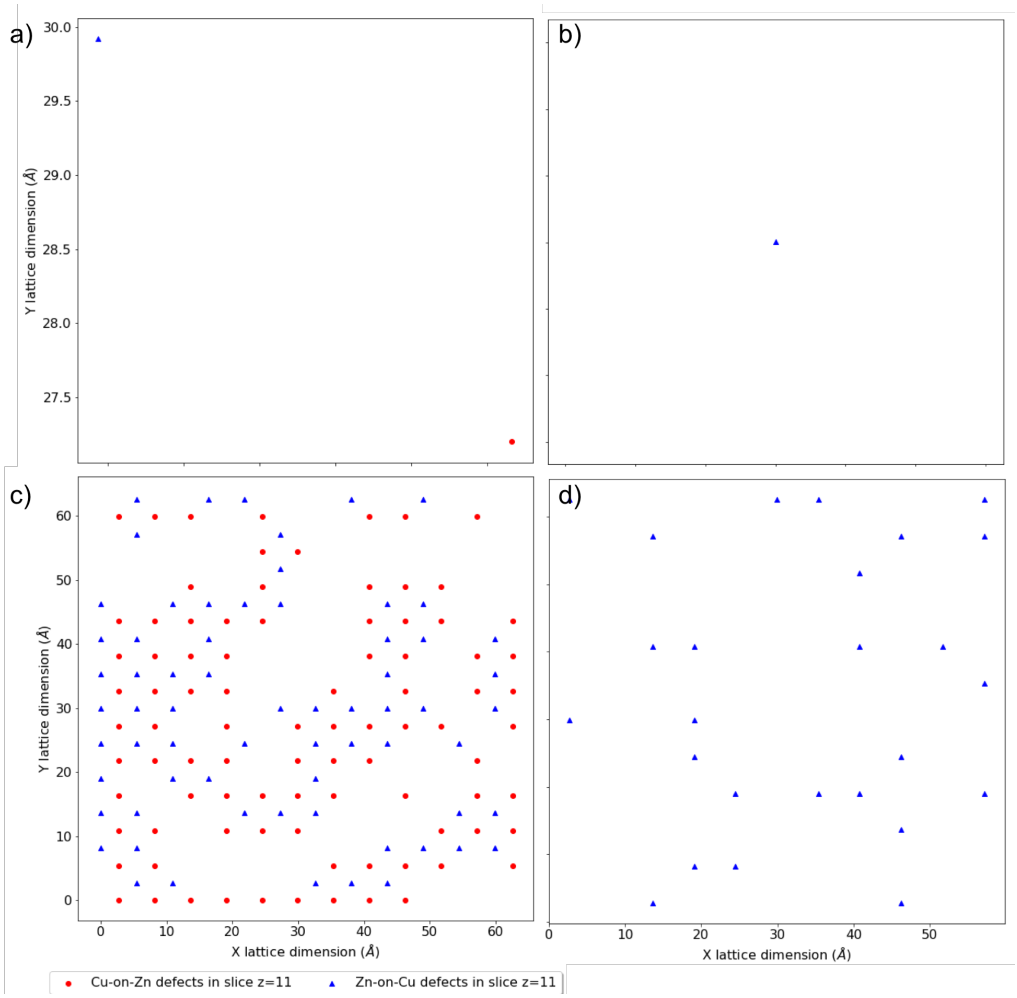

Fig. 9 24×24×24 ions system with 3D Cu/ Zn disorder. Critical temperature, T_c, for the order-disorder transition is approximately 650K for this system. (a) and (b) show antisite locations at T=400K in a Cu-Zn and Cu-Sn plane respectively. (c) and (d) show the same for T=750K, i.e. above and below T_c respectively.

4 Summary and further work

In summary, we have developed a Monte Carlo model to simulate Cu/ Zn disorder in kesterite-structured Cu_2ZnSnS_4 based on electrostatic pairwise interactions and parameterised with the bulk dielectric constant of Cu_2ZnSnS_4 from first principles calculations. Cu/ Zn disorder between 2*c* and 2*d* sites is believed to be the most prevalent type of substitutional disorder for near stoichiometric samples [18]. However recent studies have suggested that disorder is also prevalent on the 2*a* site [33,34]. We simulate separately 2D and 3D Cu/ Zn disorder. For the former the only disorder mechanism present is substitutions between Cu and Zn ions on 2*c* and 2*d* Wyckoff sites. For the 3D disorder process, Zn may also substitute onto the Cu 2*a* sites.

We find that the order-disorder transition (ODT) critical temperature (T_C) is lower for full 3D Cu/ Zn disorder compared to the 2D mechanism alone, taking T_C of the model closer to that observed experimentally. In line with other recent works [33,34], our model suggests that it is important to also consider Cu/ Zn disorder on the Cu 2*a* sites to gain atomistic insights into Cu/ Zn disorder in this promising PV material. Extending the Monte Carlo procedure to treat off-stoichiometric kesterites, as are often found to produce the highest-performing devices, and incorporating the effects of disorder on electron transport and recombination in kesterite solar cells will be a valuable line for future research.

5 Data access statement

The Monte Carlo model is implemented in the code ERIS, which is available from https://doi.org/10.5281/zenodo.1248445 under an MIT open-source license. **PUSH LATEST VERSION OF CODE TO MASTER BRANCH FOR NEW RELEASE** Data from our Monte Carlo simulations is available from the online repository ZENODO at **UPLOAD DATA TO ZENODO**

6 Acknowledgements

We thank Laurie Peter, Mark Weller, David Mitzi, and Benjamin Morgan for useful discussions. This research has been funded by the EPSRC (Grant No. EP/L017792/1 and EP/K016288/1), as well as the EU Horizon2020 Framework (STARCELL, Grant No. 720907). AW is supported by a Royal Society University Research Fellowship. We are grateful to the UK Materials and Molecular Modelling Hub for computational resources, which is partially funded by EPSRC (EP/P020194/1).

References

1 X. Liu, Y. Feng, H. Cui, F. Liu, X. Hao, G. Conibeer, D. B. Mitzi and M. Green, *Progress in Photovoltaics: Research and Applications*, 2016, **24**, 879–898.
2 W. Shockley and H. J. Queisser, *Journal of Applied Physics*, 1961, **32**, 510.
3 W. Wang, M. T. Winkler, O. Gunawan, T. Gokmen, T. K. Todorov, Y. Zhu and D. B. Mitzi, *Advanced Energy Materials*, 2013, **4**, 1301465.
4 C. Yan, J. Huang, K. Sun, S. Johnston, Y. Zhang, H. Sun, A. Pu, M. He, F. Liu, K. Eder, L. Yang, J. M. Cairney, N. J. Ekins-Daukes, Z. Hameiri, J. A. Stride, S. Chen, M. A. Green and X. Hao, *Nature Energy*, 2018, **3**, 764–772.
5 P. Jackson, R. Wuerz, D. Hariskos, E. Lotter, W. Witte and M. Powalla, *physica status solidi (RRL) - Rapid Research Letters*, 2016, **10**, 583–586.
6 S. Bourdais, C. Choné, B. Delatouche, A. Jacob, G. Larramona, C. Moisan, A. Lafond, F. Donatini, G. Rey, S. Siebentritt, A. Walsh and G. Dennler, *Advanced Energy Materials*, 2016, **6**, 1502276.
7 R. Aninat, L.-E. Quesada-Rubio, E. Sanchez-Cortezon and J.-M. Delgado-Sanchez, *Thin Solid Films*, 2017, **633**, 146 – 150.
8 S. K. Wallace, D. B. Mitzi and A. Walsh, *ACS Energy Letters*, 2017, **2**, 776–779.
9 J. Li, D. Wang, X. Li, Y. Zeng and Y. Zhang, *Advanced Science*, 2018, 1700744.
10 T. K. Todorov, K. B. Reuter and D. B. Mitzi, *Advanced Materials*, 2010, **22**, E156–E159.
11 T. Gokmen, O. Gunawan, T. K. Todorov and D. B. Mitzi, *Applied Physics Letters*, 2013, **103**, 103506.
12 L. L. Baranowski, P. Zawadzki, S. Lany, E. S. Toberer and A. Zakutayev, *Semiconductor Science and Technology*, 2016, **31**, 123004.
13 S. Lany, A. N. Fioretti, P. P. Zawadzki, L. T. Schelhas, E. S. Toberer, A. Zakutayev and A. C. Tamboli, *Physical Review Materials*, 2017, **1**, 035401.
14 S. Chen, J.-H. Yang, X. G. Gong, A. Walsh and S.-H. Wei, *Physical Review B*, 2010, **81**, 245204.
15 S. Schorr, *Solar Energy Materials and Solar Cells*, 2011, **95**, 1482–1488.
16 T. Washio, H. Nozaki, T. Fukano, T. Motohiro, K. Jimbo and H. Katagiri, *Journal of Applied Physics*, 2011, **110**, 074511.
17 B. G. Mendis, M. D. Shannon, M. C. Goodman, J. D. Major, R. Claridge, D. P. Halliday and K. Durose, *Progress in Photovoltaics: Research and Applications*, 2012, **22**, 24–34.
18 D. M. Többens, G. Gurieva, S. Levcenko, T. Unold and S. Schorr, *physica status solidi (b)*, 2016, **253**, 1890–1897.
19 J. J. S. Scragg, L. Choubrac, A. Lafond, T. Ericson and C. Platzer-Björkman, *Applied Physics Letters*, 2014, **104**, 041911.
20 G. Rey, A. Redinger, J. Sendler, T. P. Weiss, M. Thevenin, M. Guennou, B. E. Adib and S. Siebentritt, *Applied Physics Letters*, 2014, **105**, 112106.
21 A. Ritscher, M. Hoelzel and M. Lerch, *Journal of Solid State Chemistry*, 2016, **238**, 68–73.
22 G. Rey, T. Weiss, J. Sendler, A. Finger, C. Spindler, F. Werner, M. Melchiorre, M. Hála, M. Guennou and S. Siebentritt, *Solar Energy Materials and Solar Cells*, 2016, **151**, 131 – 138.
23 K. Rudisch, Y. Ren, C. Platzer-Björkman and J. Scragg, *Applied Physics Letters*, 2016, **108**, 231902.
24 K. Yu and E. A. Carter, *Chemistry of Materials*, 2016, **28**, 864–869.
25 A. Polizzotti, I. L. Repins, R. Noufi, S.-H. Wei and D. B. Mitzi, *Energy & Environmental Science*, 2013, **6**, 3171.
26 S. Siebentritt, *Nature Energy*, 2017, **2**, 840–841.
27 K. Sun, C. Yan, F. Liu, J. Huang, F. Zhou, J. A. Stride, M. Green and X. Hao, *Advanced Energy Materials*, 2016, **6**, 1600046.
28 M. A. Lloyd, D. Bishop, O. Gunawan and B. McCandless, 2016 IEEE 43rd Photovoltaic Specialists Conference (PVSC), 2016.
29 P. Zawadzki, A. Zakutayev and S. Lany, *Physical Review B*, 2015, **92**, 201204.
30 P. Zawadzki, A. Zakutayev and S. Lany, *Physical Review Applied*, 2015, **3**, 034007.
31 J. J. S. Scragg, J. K. Larsen, M. Kumar, C. Persson, J. Sendler, S. Siebentritt and C. P. Björkman, *physica status solidi (b)*, 2015, **253**, 247–254.
32 S. Shang, Y. Wang, G. Lindwall, N. R. Kelly, T. J. Anderson and Z.-K. Liu, *The Journal of Physical Chemistry C*, 2014, **118**, 24884–24889.
33 S. P. Ramkumar, A. Miglio, M. J. van Setten, D. Waroquiers, G. Hautier and G.-M. Rignanese, *Phys. Rev. Materials*, 2018, **2**, 085403.
34 C. J. Bosson, M. T. Birch, D. P. Halliday, K. S. Knight, A. S. Gibbs and P. D. Hatton, *Journal of Materials Chemistry A*, 2017, **5**, 16672–16680.
35 O. Tange, *The USENIX Magazine*, 2011, **36**, 42–47.
36 K. Momma and F. Izumi, *Journal of Applied Crystallography*, 2011, **44**, 1272–1276.
37 T. Shibuya, J. M. Skelton, A. J. Jackson, K. Yasuoka, A. Togo, I. Tanaka and A. Walsh, *APL Materials*, 2016, **4**, 104809.
38 J. D. Gale and A. L. Rohl, *Molecular Simulation*, 2003, **29**, 291–341.
39 M. Quennet, A. Ritscher, M. Lerch and B. Paulus, *Journal of Solid State Chemistry*, 2017, **250**, 140 – 144.
40 N. Metropolis, A. W. Rosenbluth, M. N. Rosenbluth, A. H. Teller and E. Teller, *Journal of Chemical Physics*, 1953, **21**, 1087–1092.
41 B. Monserrat, J.-S. Park, S. Kim and A. Walsh, *Applied Physics Letters*, 2018, **112**, 193903.
42 E. I. Parkhomenko, *Piezoelectric and Pyroelectric Effects in Minerals*, Springer US, 1971.
43 M. E. J. Newman and G. T. Barkema, *The Ising Model and the Metropolis Algorithm*, Oxford University Press, 1999.
44 T. Gershon, D. Bishop, P. Antunez, S. Singh, K. W. Brew, Y. S. Lee, O. Gunawan, T. Gokmen, T. Todorov and R. Haight, *Current Opinion in Green and Sustainable Chemistry*, 2017, **4**, 29–36.
45 W. L. Bragg and E. J. Williams, *Proceedings of the Royal Society A: Mathematical, Physical and Engineering Sciences*, 1934, **145**, 699–730.
46 W. L. Bragg and E. J. Williams, *Proceedings of the Royal Society A: Mathematical, Physical and Engineering Sciences*, 1935, **151**, 540–566.

47 E. J. Williams, *Proceedings of the Royal Society A: Mathematical, Physical and Engineering Sciences*, 1935, **152**, 231–252.
48 P. Bais, M. T. Caldes, M. Paris, C. Guillot-Deudon, P. Fertey, B. Domengès and A. Lafond, *Inorganic Chemistry*, 2017, **56**, 11779–11786.
49 A. Ritscher, A. Franz, S. Schorr and M. Lerch, *Journal of Alloys and Compounds*, 2016, **689**, 271–277.